Anshu Nagar, *Richa Sharma*[*]

FRACTURE ANALYSIS OF HEMISPHERICAL DENTAL IMPLANT CROWNS COMPOSED OF FUNCTIONALLY GRADED TRANSVERSELY ISOTROPIC MATERIAL UNDER EXTERNAL PRESSURE

ANALIZA LOMA POLUSFERNIH ZUBNIH KRUNICA IMPLANTATA OD FUNKCIONALNOG KOMPOZITNOG TRANSVERZALNOG IZOTROPNOG MATERIJALA POD DEJSTVOM SPOLJAŠNJEG PRITISKA

Originalni naučni rad / Original scientific paper
Rad primljen / Paper received: 15.07.2024
https://doi.org/10.69644/ivk-2025-siA-0085

Adresa autora / Author's address:
Jaypee Institute of Information Technology, Noida (Uttar Pradesh), India, [*]email: richa.ggit@gmail.com

Keywords
- dental implant crowns
- functionally-graded materials
- transversely isotropic material
- hemispherical shells, plastic theory
- transition theory

Ključne reči
- zubne krunice implantata
- funkcionalni kompozitni materijali
- transverzalni izotropni materijal
- polusferne ljuske, teorija plastičnosti
- teorija prelaznih napona

Abstract

Dental implants are artificial teeth surgically inserted into a person's jaw to restore their chewing ability or look. They support prosthetic teeth, such as crowns, bridges, and dentures. In this paper, the crown part of a dental implant system in the shape of a hemispherical shell composed of functionally graded transversely isotropic material is considered. The idea of transition theory has been employed to evaluate transitional and plastic stresses in the shell under external pressure, and the obtained results are used to compare the strength and compatibility of zirconia and titanium-based crowns. Resulting relations are substituted in the equilibrium equation to create a nonlinear differential equation that regulates this physical problem of the dental implant crown. For estimating transitional stresses and pressure in the shell, the transition function R in the form of radial stress T_{rr} is considered, and the analytical method is applied to solve equations by taking the critical point $P \to \pm\infty$ of the governing differential equation into consideration. The study examines a crown composed of FG transversely isotropic material more robust and biocompatible than homogenous transversely isotropic material. With the use of graphs and numerical computations, it is observed that functionally graded transversely isotropic material zirconia with $k = 3$ has the highest circumferential stresses and lowest radial stresses. Therefore, it can be concluded that zirconia dental implants, known as ceramic implants are more suitable than titanium dental implants due to their excellent aesthetic properties and biocompatibility.

Izvod

Zubni implantati su veštački zubi koji se hirurški uvode u vilicu kako bi se omogućilo žvakanje ili zbog estetike. Oni treba da nose zubnu protetiku, na pr. krunice, mostove i proteze. U radu se razmatra krunica u konstrukciji zubnog implantata, oblika polusferne ljuske, izrađena od funkcionalnog kompozitnog transverzalno izotropnog materijala. Sa idejom uvođenja teorije prelaznih napona, proračunavaju se prelazni i naponi plastičnog stanja u ljusci pod dejstvom pritiska, a dobijeni rezultati se upoređuju sa kompatibilnošću i čvrstoćom krunice na bazi cirkonijum oksida i titanijuma. Dobijene relacije unose se smenom u jednačinu ravnoteže, kako bi se dobila nelinearna diferencijalna jednačina koja opisuje ovaj fizički problem krunice zubnog implantata. Za procenu prelaznih napona i pritiska u ljusci, razmatra se prelazna funkcija R oblika radijalnog napona T_{rr}, a primenjuje se analitička metoda za rešavanje jednačina uzimanjem u obzir kritične tačke $P \to \pm\infty$ date jednačine. Istraživanja obuhvataju krunicu od FG transverzalno izotropnog materijala, koji je izdržljiviji sa boljom biokompatibilnošću u odnosu na homogeni transverzalni izotropni materijal. Upotrebom dijagrama i numeričkog proračuna, uočava se da funkcionalni kompozitni transverzalno izotropni materijal, tj. oksid cirkonijuma sa $k = 3$ ima najveće obimske napone i najmanje radijalne napone u odnosu na titanijum. Stoga se može zaključiti da su zubni implantati od oksida cirkonijuma, poznati i kao keramički implantati pogodniji u odnosu na zubne implantate od titanijuma, zbog njihovih izvanrednih osobina biokompatibilnosti i estetike.

INTRODUCTION

Dental implants have gained popularity with the evolution of technology in dental field. Dental implants enable people to chew, bite, and talk confidently while also restoring the natural functionality of their teeth. They are intended to closely imitate natural teeth, creating a smooth and natural-looking smile. They are customized to complement colour, shape, and size of surrounding teeth, resulting in a harmonious look. Dental implant crowns are extremely durable and can endure for many years if properly maintained. Unlike other dental alternatives, they do not require any specific maintenance or repairs, thus makes them a long-term cost-effective choice. However, the materials used for dental implant crowns must be carefully selected to provide aesthetic appeal, longevity, and compatibility with the neighbouring teeth. Here are the most popular options for dental implants: ceramic crowns such as porcelain crowns, metal crowns, zirconia-based crowns, metal-free crowns such as titanium crowns. Common biocompatible materials include porcelain, zirconia, and metal alloys. Dental implant crowns are subject to significant biting forces and constant use, so their durability is of utmost importance. Different materials have varying levels of strength and resistance to wear. For instance, zirconia is known for exceptional durability, whereas porcelain may be more prone to chipping or cracking.

Spherical shell structures are widely used in variety of industrial applications, including hemispherical resonator gyroscopes, energy harvesters. The hemispherical shell is half of the spherical shell, hence the model is structurally sturdier for use in the actual structure than the perfect shell, for example in dental implant crowns. The material's strength plays an essential role for all of these applications. Historically, homogenous materials were utilised to make shells, but current researchers are intrigued by functionally graded materials due to their different mechanical properties. FGMs are advanced composite substances designed to endure temperatures that are extremely high and are used in technological applications such as aerospace, medicine, defence, energy and optoelectronics. Pompea and others /1/ investigated that living tissues, such as bones and teeth, are classified as functionally graded materials from nature. In order to replace these tissues, a compatible material is required that will serve the same purpose as the original bio-tissue and the best alternative for this application is functionally graded material. Matsuo et al. /2/ applied laser lithography to fabricate functionally graded dental composite resin posts and cores and finite element method for stress analysis and found FGM has wide used in dental field. Watari et al. /3/ described how FGM were developed for biomedical applications, particularly implant applications, and found FGM is best alternative for teeth and bone replacement. Zou et al. /4/ considered elastic spherical shells as research objects for the underwater vibro-acoustic problems of structures coupled with nonlinear systems and obtained the vibration response without time-domain acoustic field solution. Ye et al. /5/ investigated multilayered FG spherical shells with basic boundary constraints with the use of three-dimensional form of shell theory of elasticity and compared results acquired by approximate numerical methods. Chu et al. /6/ employed chemical etching method to investigate the impact of SSD removal on the Q factor variation and found chemical etching may efficiently eliminate the SSD from the surface of the fused hemispherical silica resonator, while also greatly improving the Q factor. Xu et al. /7/ discovered a dynamic model of an inadequate hemispherical shell resonator and analysed output error in it and demonstrated the impact of frequency splitting on HRG output inaccuracy. Xu et al. /8/ discovered a thermoelastic model of a hemispherical shell under variable temperatures and found it suitable for accurate error analysis. Amabili et al. /9/ developed a nonlinear theory for circular cylinder shells formed of incompressible hyper elastic materials and compared the solutions obtained by higher-order shear deformation theory. Beheshti et al. /10/ employed a higher-order shell theory for the significant deformation of shells formed of transversely isotropic materials and investigated various instances to demonstrate the functionality of the suggested elements in addition to anisotropy effects.

To describe the fracture properties of piezoelectric materials, Tan et al. /11/ developed a unique phase field computational framework with a temperature effect and found it useful for the future design of piezoelectric devices in practical engineering. Mehta et al. /12/ discovered the stress analysis of FGM disc and demonstrated that the disc with a quadratic temperature profile expands more than the disc with the linear temperature profile and found that a disc with a quadratic temperature profile performs better than a disc with a linear temperature variation. Shi and Xie /13/ evaluated the analytical solutions of stress and displacement fields of the FG cylinder under internal pressure and compared the results with the existing results of related simplified problems. Kholdi et al. /14/ studied the stress analysis of a rotating annular disc formed of FGMs using Successive Approximation Method (SAM) and found increasing the percentage of ceramic particles in the outer layers of the cylinder's wall reduces the plastic strains in those layers, while increasing the number of plastic strains and the range of plastic region in interior thickness layers. Bagheri et al. /15/ investigate the dynamic stress intensity parameters of multiple moving cracks with arbitrary patterns placed along the FGP strip by using a distributed dislocation approach and used graphs to present the trend of both factors: stress intensity and electric displacement intensity. Sharma et al. /16-17/ investigated creep stresses in transversely isotropic cylinder having thick walls formed of FGM with internal and external pressure and found that both rotation and non-homogeneity have a considerable impact on thermal creep strains. Chand et al. /18/ evaluated the stresses in an annular isotropic disc under internal pressure and found hoop stress is highest near the compressible material disc’s outer surface, in contrast to incompressible material. Godana et al. /19/ used Seth’s mid-zone idea to generalized strain measure theory for modelling elastoplastic deformation in a transversely isotropic shell under temperature gradient and consistent pressure and found the stress distribution over the surface of the shell. Shahi /20/ employed Seth’s transition concept to evaluate stresses in a hemispherical shell formed of transversely isotropic material for dental implant crown and found zirconia is a better option for crown part of dental implant. Sharma /22/ evaluated the stresses in a thin annular transversely isotropic piezoelectric disk with variable thickness and density using mid-zone theory and found that a disk made of barium titanate $BaTiO_3$ (piezoelectric) performs better than a disk made of PZT4 (piezoceramic). Sharma and Nagar /23/ employed analytic approach to evaluate the stresses in an FG piezoelectric disc with variable compressibility and variable density and found that annular disc made of PZT-4 is better for the purpose of engineering designs.

In all the above studies, elastic-plastic and creep stresses are evaluated for different structures as elastic spherical shells, circular cylinders, an imperfect hemispherical shell, an annular isotropic disc, a thick-walled cylinder formed of different materials as FG isotropic, FG transversely isotropic, incompressible hyper elastic, etc., under different conditions, i.e., pressure and temperature using shell theory, classical theory, and transition theory. But no one evaluated elastic-plastic stresses for FG transversely isotropic hemispherical shell using transition theory.

The objective of this research is to examine the strength of dental implant crown in the form of hemispherical shell composed of FG transversely isotropic material. Transitional and plastic stresses are evaluated in a hemispherical shell of FG transversely isotropic material subjected to external pressure. In the present problem, the dental crown composed of FG transversely isotropic material is considered which is a novelty of this research. Dental crowns of FG transversely isotropic material (titanium and zirconia) are compared based on biocompatibility and durability of the crowns.

MATHEMATICAL FORMULATION

Consider a hemispherical shell with inner- and outer radius as r_1 and r_2, respectively, under uniaxial external pressure p with constant thickness and variable compressibility, Figs. 1 and 2. The external pressure acts radially to simulate the state of axial compression.

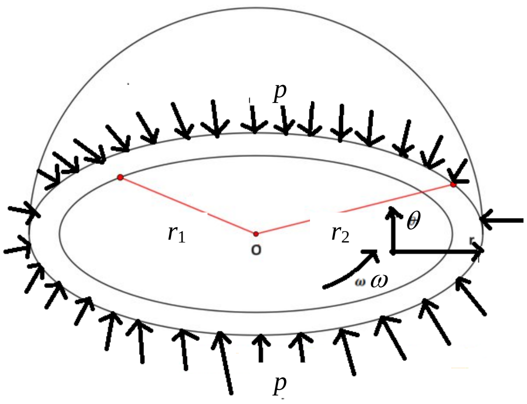

Figure 1. Geometry of hemispherical shell with external pressure.

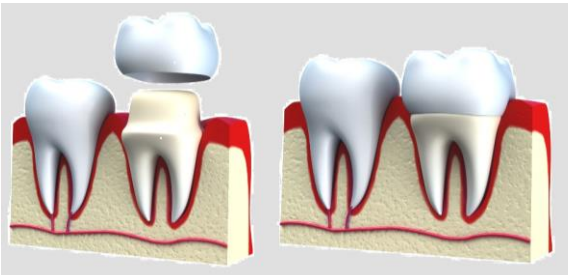

Figure 2. Structure of dental implant crown in the form of hemispherical shell.

In the form of spherical coordinates (r, θ, φ) the displacement coordinates u and v are considered to be

$$u = r(1-\beta), \quad v = 0 \quad \text{(Borah /21/)}, \tag{1}$$

where: $\beta = [\beta(r)]$ is a function of r; and $r = \sqrt{(x^2 + y^2)}$.

Using the generalised strain measure /21/, the strain components are given as

$$e_{rr} = \frac{1}{n}[1-(r\beta'+\beta)^n] = \frac{1}{n}[1-\beta^n(1+P)^n],$$
$$e_{\theta\theta} = e_{\varphi\varphi} = \frac{1}{n}[1-\beta^n], \tag{2}$$

where: strain measure is n; and $\beta' = d\beta/dr$.

Stress-strain relationships for transversely isotropic materials by Hooke's law are given as:

$$T_{rr} = c_{33}e_{rr} + 2c_{12}e_{\theta\theta},$$
$$T_{\theta\theta} = c_{12}e_{rr} + 2(c_{11}-c_{66})e_{\theta\theta},$$
$$T_{r\theta} = T_{\theta\varphi} = T_{\varphi r} = 0. \tag{3}$$

Substituting Eq.(2) into Eq.(3), the stresses are:

$$T_{rr} = \frac{c_{33}}{n}[1-\beta^n(1+P)^n] + \frac{2c_{12}}{n}[1-\beta^n],$$
$$T_{\theta\theta} = T_{\varphi\varphi} = \frac{c_{21}}{n}[1-\beta^n(1+P)^n] + \frac{2(c_{11}-c_{66})}{n}[1-\beta^n], \tag{4}$$

where: $r\beta' = \beta P$ (P is function of β, and β is function of r).

For functionally graded properties of the transversely isotropic material, the compressibility of the shell is assumed to be varied radially,

$$c_{11} = c_{011}\left(\frac{r}{r_2}\right)^k, \quad c_{66} = c_{066}\left(\frac{r}{r_2}\right)^k, \quad c_{12} = c_{012}\left(\frac{r}{r_2}\right)^k. \tag{5}$$

Using Eqs. (4) and (5), the stresses are given as

$$T_{rr} = \frac{c_{033}}{n}\left(\frac{r}{r_2}\right)^k[1-\beta^n(1+P)^n] + \frac{2c_{012}}{n}\left(\frac{r}{r_2}\right)^k[1-\beta^n],$$
$$T_{\theta\theta} = T_{\varphi\varphi} = \frac{c_{021}}{n}\left(\frac{r}{r_2}\right)^k[1-\beta^n(1+P)^n] +$$
$$+\frac{2(c_{011}-c_{066})}{n}\left(\frac{r}{r_2}\right)^k[1-\beta^n]. \tag{6}$$

Equations of equilibrium for the shell are as follows:

$$\frac{\partial T_{rr}}{\partial r} + \frac{1}{r\sin\theta}\frac{\partial T_{r\varphi}}{\partial\varphi} + \frac{1}{r}\frac{\partial T_{r\theta}}{\partial\theta} + \frac{2T_{rr}-T_{\theta\theta}-T_{\varphi\varphi}+T_{r\theta}\cot\theta}{r} = 0,$$
$$\frac{\partial T_{r\theta}}{\partial r} + \frac{1}{r\sin\theta}\frac{\partial T_{\theta\varphi}}{\partial\varphi} + \frac{1}{r}\frac{\partial T_{\theta\theta}}{\partial\theta} + \frac{3T_{r\theta}+(T_{\theta\theta}-T_{\varphi\varphi})\cot\theta}{r} = 0,$$
$$\frac{\partial T_{r\varphi}}{\partial r} + \frac{1}{r\sin\theta}\frac{\partial T_{\varphi\varphi}}{\partial\varphi} + \frac{1}{r}\frac{\partial T_{\varphi\theta}}{\partial\theta} + \frac{3T_{r\varphi}+2T_{\theta\theta}\cot\theta}{r} = 0. \tag{7}$$

Substituting Eq.(6) into Eq.(7), we observe that all the equilibrium equations are satisfied except:

$$\frac{\partial T_{rr}}{\partial r} - \frac{2(T_{rr}-T_{\theta\theta})}{r} = 0. \tag{8}$$

Equation (8) may also result in the conclusion that

$$T_{\varphi\varphi} - T_{\theta\theta} = 0. \tag{9}$$

By putting the values of T_{rr} and $T_{\theta\theta}$ from Eq.(6) into Eq.(8), the governing differential equation is obtained as

$$\beta^{n+1}P(P+1)^{n-1}\frac{dP}{d\beta} = \frac{r}{n}\left[\frac{k}{r}(1-\beta^n(P+1)^n) - \frac{n}{r}\beta^n P(P+1)^n\right] + \frac{2r}{n}(1-C_1)\left[-\frac{n}{r}\beta^n P + \frac{k}{r}(1-\beta^n)\right] + \frac{2}{n}[(1-\beta^n(P+1)^n)C_1 + 2(1-\beta^n)C_2] \tag{10}$$

where: $C_1 = (c_{033} - c_{012})/c_{033}$, $C_2 = (c_{012} - c_{011} + c_{066})/c_{033}$.

The interior and exterior surfaces of the hemispherical shell are assumed to have boundary conditions as follows:

$$T_{rr} = 0 \quad \text{at} \quad r = r_1,$$
$$T_{rr} = -p \quad \text{at} \quad r = r_2. \tag{11}$$

TRANSITION FROM ELASTIC TO PLASTIC STATE

Seth's mid-zone theory states that the transition from elastic to plastic takes place at transformation point $P \to \pm\infty$ /21/. For estimating transitional and plastic stresses, the transition function R is considered in the form of radial stress T_{rr} as

$$R=(3-2C_1)-\frac{nT_{rr}}{c_{33}}=(3-2C_1)-(1-\beta^n(1+P)^n)-2(1-C_1)(1-\beta^n)\,, \tag{12}$$

where: c_{33} is any constant.

Taking logarithmic differentiation of Eq.(12) with respect to r, we get

$$\frac{d\log R}{dr}=\frac{\frac{n}{r}\beta^{n+1}P(P+1)^{n-1}\frac{dP}{d\beta}+\frac{n}{r}\beta^n P(P+1)^n+\frac{2n}{r}(1-C_1)\beta^n P}{(3-2C_1)-(1-\beta^n(1+P)^n)-2(1-C_1)(1-\beta^n)}\,. \tag{13}$$

Putting $dP/d\beta$ value from Eq.(10), we get

$$\frac{d\log R}{dr}=\frac{\frac{k}{r}(1-\beta^n(P+1)^n)+\frac{2k}{r}(1-C_1)(1-\beta^n)+\frac{2}{r}[(1-\beta^n(P+1)^n)C_1+2(1-\beta^n)C_2]}{(3-2C_1)-(1-\beta^n(1+P)^n)-2(1-C_1)(1-\beta^n)}\,, \tag{14}$$

and then employing the transition point $P\to\pm\infty$ and integrating we get

$$R=Ar^{-(k+2C_1)}\,, \tag{15}$$

where: A is the integration constant.

Equating Eqs. (10) and (11), and then by substituting the value of T_{rr} in Eq.(7), we get stresses as:

$$T_{rr}=\frac{c_{033}}{n}\left(\frac{r}{r_2}\right)^k\left((3-2C_1)-Ar^{-(k+2C_1)}\right). \tag{16}$$

Using boundary conditions, Eq.(11), we get

$$A=\frac{3-2C_1}{r_1^{-(k+2C_1)}},\quad p=\frac{-(3-2C_1)}{n}c_{033}\left[1-\left(\frac{r_2}{r_1}\right)^{-(k+2C_1)}\right]. \tag{17}$$

Substituting Eq. (17) in Eq. (16), we get

$$T_{rr}=\frac{(3-2C_1)}{n}c_{033}\left(\frac{r}{r_2}\right)^k\left(1-\left(\frac{r}{r_1}\right)^{-(k+2C_1)}\right). \tag{18}$$

Using Eq.(17) in equation of equilibrium, Eq.(7), we get

$$T_{\theta\theta}=T_{rr}+\frac{r(3-2C_1)}{2n}c_{033}\left[\frac{k}{r}\left(\frac{r}{r_2}\right)^k\left(1-\left(\frac{r}{r_1}\right)^{-(k+2C_1)}\right)+(k+2C_1)\left(\frac{r}{r_2}\right)^k\left(\frac{r}{r_1}\right)^{-(k+2C_1)}\right]. \tag{19}$$

Initial yielding emerges at the shell's exterior surface, as a result, Eq.(19) at $r = r_2$ yields

$$\left|T_{\theta\theta}-T_{rr}\right|_{r=r_2}=Y_1\,,\qquad Y_1=\left|\frac{r(3-2C_1)}{2n}c_{033}\left[\frac{k}{r_2}\left(1-\left(\frac{r_2}{r_1}\right)^{-(k+2C_1)}\right)+(k+2C_1)\left(\frac{r_2}{r_1}\right)^{-(k+2C_1+1)}\right]\right|. \tag{20}$$

For the state of fully plastic ($C_1\to 0$), Eq.(20) becomes

$$Y_2=\left|\frac{3r_2}{2n}c_{033}\left[\frac{k}{r_2}\left(1-\left(\frac{r_2}{r_1}\right)^{-k}\right)+k\left(\frac{r_2}{r_1}\right)^{-(k+1)}\right]\right|. \tag{21}$$

We present the following non-dimensional components as

$$R=\frac{r}{r_1},\quad R_0=\frac{r_2}{r_1},\quad \sigma_{r1}=\frac{T_{rr}}{Y_1},\quad \sigma_{\theta1}=\frac{T_{\theta\theta}}{Y_1},\quad \sigma_{r2}=\frac{T_{rr}}{Y_2},\quad \sigma_{\theta2}=\frac{T_{\theta\theta}}{Y_2},\quad p_i=\frac{p}{Y_1},\quad p_f=\frac{p}{Y_2}\,. \tag{22}$$

Using Eqs. (16) and (19), the transitional and plastic stresses in non-dimensional manner can be stated as

$$\sigma_{r1}=\frac{(R/R_0)^k\left(1-R^{-(k+2C_1)}\right)}{r_2\left[\frac{k}{r_2}\left(1-R_0^{-(k+2C_1)}\right)+(k+2C_1)R_0^{-(k+2C_1+1)}\right]},\quad \sigma_{\theta1}=\frac{(R/R_0)^k\left(1-R^{-(k+2C_1)}\right)(1+k)+r_2(k+2C_1)(R/R_0)^k R^{-(k+2C_1+1)}}{r_2\left[\frac{k}{r_2}\left(1-R_0^{-(k+2C_1)}\right)+(k+2C_1)R_0^{-(k+2C_1+1)}\right]},$$

$$\sigma_{r2}=\frac{2(R/R_0)^k(1-R^{-k})}{r_2\left[\frac{k}{r_2}(1-R_0^{-k})+kR_0^{-(k+1)}\right]},\quad \sigma_{\theta2}=\frac{(R/R_0)^k(1-R^{-k})(2+k)+kr_2(R/R_0)^{k+1}R^{-(k+1)}}{r_2\left[\frac{k}{r_2}(1-R_0^{-k})+kR_0^{-(k+1)}\right]}\,. \tag{23}$$

Initial pressure in a non-dimensional form may be described as

$$p_i=\frac{-\frac{2}{r_2}\left(1-R_0^{-(k+2C_1)}\right)}{\frac{k}{r_2}\left(1-R_0^{-(k+2C_1)}\right)+(k+2C_1)R_0^{-(k+2C_1+1)}}\,. \tag{24}$$

Pressure required for fully plastic state in a non-dimensional form

$$p_f=\frac{-\frac{2}{r_2}(1-R_0^{-k})}{\frac{k}{r_2}(1-R_0^{-k})+kR_0^{-(k+1)}}\,. \tag{25}$$

NUMERICAL DISCUSSION

The standard values of all material constants for the considered materials are used from Table 1. To illustrate the impact of pressure on elastic plastic stress distributions, the values of parameters used in this study are selected arbitrarily. All graphs are drawn using Mathematica® software. Figures 3 to 17 represent the initial and fully plastic pressure and transitional and fully plastic stresses with different radii ratios $R = r/r_2$ in the case of the hemispherical shell of functionally graded transversely isotropic materials (titanium and zirconia) for different values of k = 1, 2, and 3, respectively.

Table 1. Material constant values of transversely isotropic materials titanium, zirconia, dentin, enamel, and HAP.

Material constant	c_{11}	c_{33}	c_{12}	c_{13}
titanium	162.7	180.7	92	69
zirconia	361	258	142	55
dentin	37	39	16.6	8.7
enamel	115	125	42.4	30
hydroxyapatite (HAP)	117.9	165	30.55	66.4

Graphs for transition state

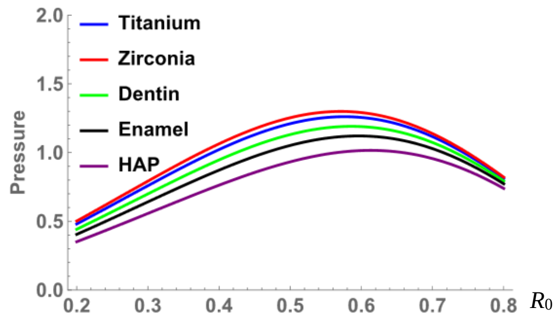

Figure 3. Initial pressure in the hemispherical crown for dental implant for k = 1.

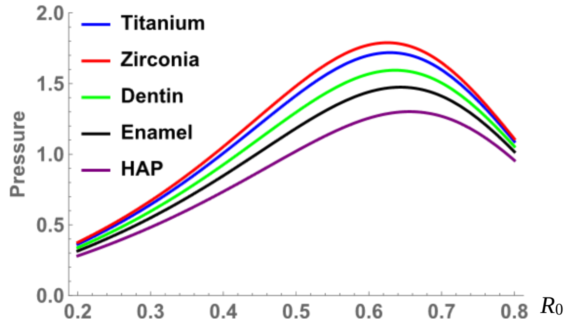

Figure 4. Initial pressure in the hemispherical crown for dental implant for k = 2.

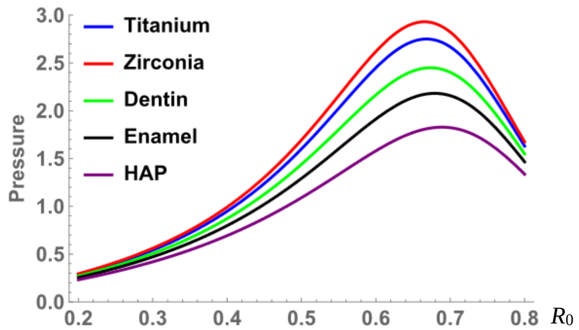

Figure 5. Initial pressure in the hemispherical crown for dental implant for k = 3.

Figures 3, 4 and 5 illustrate the pressure necessary for initial yielding in a hemispherical shell for functionally graded transversely isotropic materials (titanium and zirconia) for different values of k = 1, 2, and 3, respectively. Results are compared with standard tooth materials such as dentin, enamel, and hydroxyapatite (HAP). It can be shown that if k extends from 1 to 2, and then from 2 to 3, the values of initial pressure increase as the shell thickness increases. The value of pressure on the shell's external surface is maximum. It is also seen that pressure in the case of a zirconia shell for all three values of k is greater than pressure in the case of a shell of titanium for all three values of k.

Figures 6, 7 and 8 show the behaviour of radial stresses for initial yielding in a hemispherical crown of functionally graded transversely isotropic materials (titanium and zirconia) at different values of k = 1, 2, and 3. Results are compared with standard tooth materials such as dentin, enamel and HAP. It can be shown that stresses are maximum at the shell's outer surface and if the value of k extends from 1 to 2, and then from 2 to 3, the values of radial stresses decrease with decrease in the shell thickness. It can also be concluded that values of stresses for zirconia for all three values of k are less than values for titanium for all three values of k.

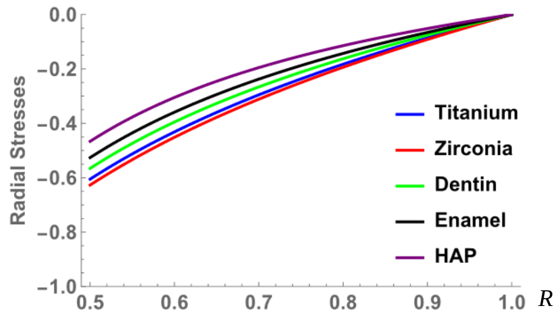

Figure 6. Radial stresses in the hemispherical crown for dental implant for k = 1.

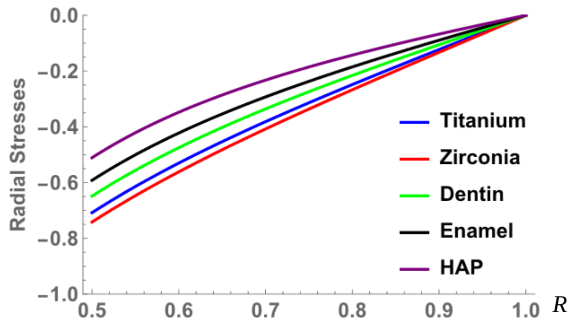

Figure 7. Radial stresses in the hemispherical crown for dental implant for k = 2.

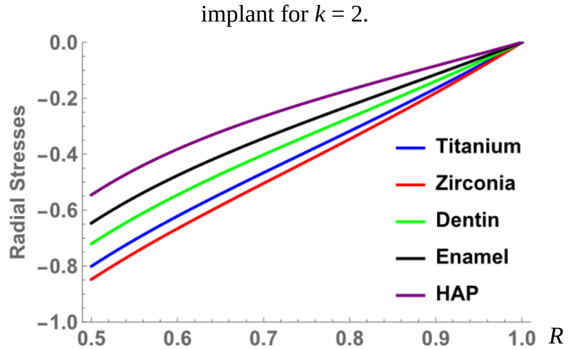

Figure 8. Radial stresses in the hemispherical crown for dental implant for k = 3.

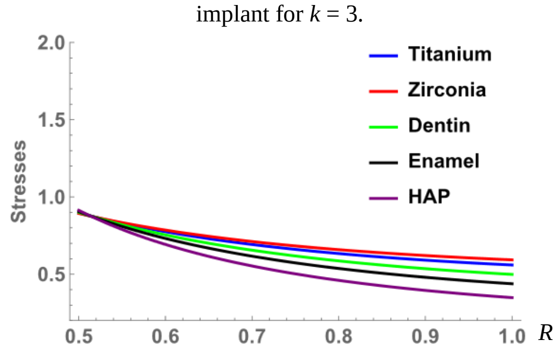

Figure 9. Circumferential stresses in the hemispherical crown for dental implant for k = 1.

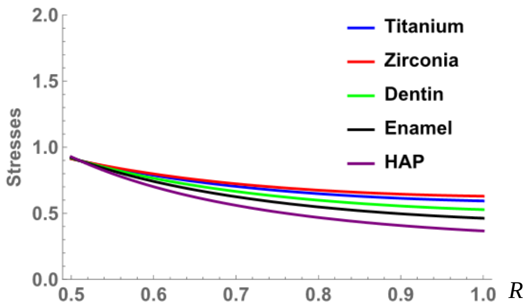

Figure 10. Circumferential stresses in the hemispherical crown for dental implant for $k = 2$.

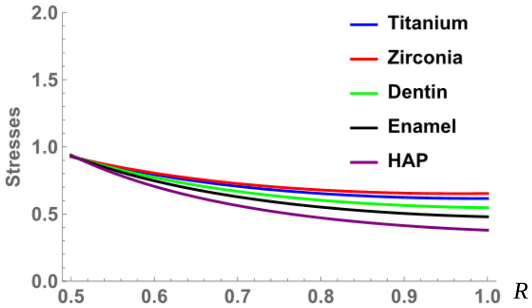

Figure 11. Circumferential stresses in the hemispherical crown for dental implant for $k = 3$.

Figures 9, 10 and 11 show the trend of circumferential stresses at initial yielding in the hemispherical shell for functionally graded transversely isotropic materials (titanium and zirconia) for different values of $k = 1$, 2, and 3, respectively. Results are compared with standard tooth materials such as dentin, enamel and HAP. It can be shown that stresses are maximum at the shell's inner surface, and if the value of k extends from 1 to 2, and then from 2 to 3, the values of circumferential stresses increase with the increase in shell thickness. It can also be concluded that values of stresses for zirconia for all three values of k are greater than the values for titanium for all three values of k.

Graphs of fully plastic state

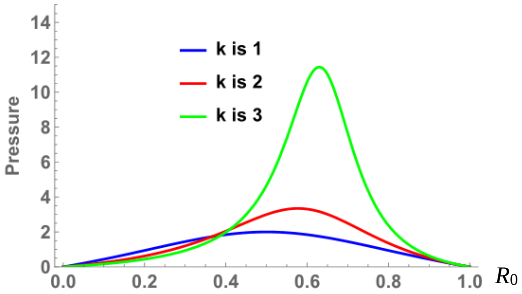

Figure 12. Pressure required at fully plastic state in the hemispherical shell with different values of k.

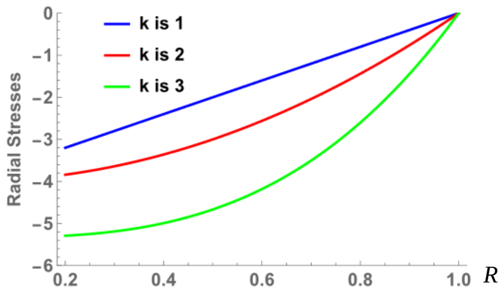

Figure 13. Radial stresses for fully plastic state in the hemispherical shell with different values of k.

Figure 12 shows the pressure needed at fully plastic state in the hemispherical shell for distinct values of k. It can be shown that pressure increases with increase in the value of compressibility parameter k of the shell.

Figure 13 shows radial stresses for fully plastic state in the hemispherical shell for different values of k. It can be shown that radial stresses increase as shell thickness increases. Also, the value of stresses for compressibility parameter $k = 1$ is greater than that for $k = 2$ and $k = 3$.

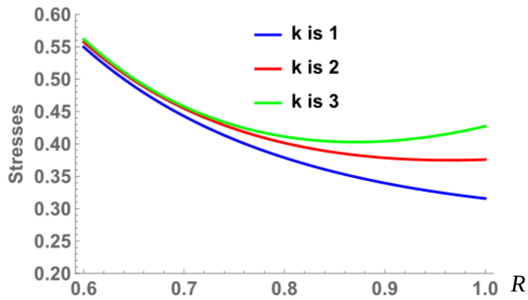

Figure 14. Circumferential stresses for fully plastic state in the hemispherical shell with different values of k.

Figure 14 shows circumferential stresses for fully plastic state in the hemispherical shell for different values of k. It can be shown that stresses decrease as shell thickness increases. Also, the value of stresses for compressibility parameter $k = 3$ is greater than that for $k = 1$ and $k = 2$.

PARTICULAR CASE (TRANSVERSELY ISOTROPIC MATERIAL)

Graphs for transition state

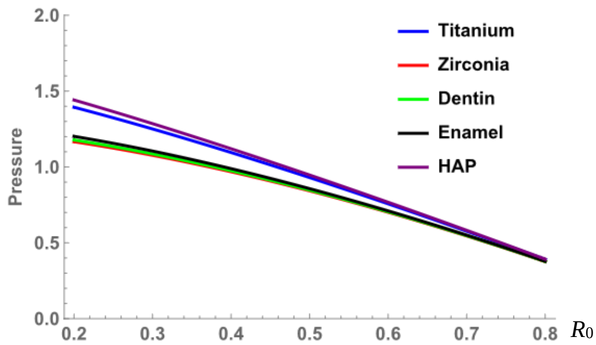

Figure 15. Initial pressure in the hemispherical crown for transversely isotropic materials.

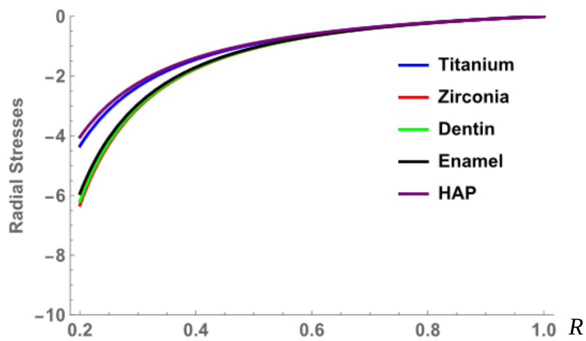

Figure 16. Radial stresses at initial yielding in the hemispherical crown for transversely isotropic materials.

Figure 15 shows the pressure needed for initial yielding in the hemispherical crown for different materials (titanium, zirconia, dentin, enamel and HAP). It can be shown that the values of initial pressure decrease as shell thickness increases. The value of pressure on the shell's external surface is minimum.

Figure 16 shows the trend of radial stresses at initial yielding in a hemispherical crown for transversely isotropic materials (titanium and zirconia). Results are compared with dentin, enamel and HAP. It can be shown that stresses are maximum at the shell's outer surface and the values of radial stresses increase as shell thickness increases.

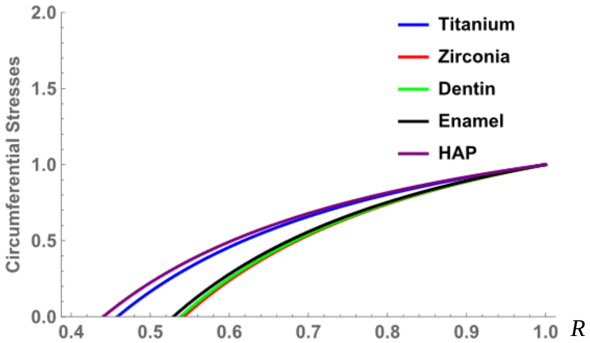

Figure 17. Circumferential stresses for initial yielding in the hemispherical crown for transversely isotropic materials.

Figure 17 shows the trend of circumferential stresses at initial yielding in a hemispherical crown for transversely isotropic materials (titanium and zirconia). Results are compared with dentin, enamel and HAP. It can be shown that stresses are maximum at the shell's outer surface and values of circumferential stresses increase as shell thickness increases.

SUMMARY AND CONCLUSION

The analytical solution is obtained for transitional and plastic stresses in a hemispherical shell composed of functionally graded transversely isotropic material with external pressure using transition theory. A comparison is made between two crowns made of functionally graded transversely isotropic materials (titanium and zirconia) to investigate which is better for a dental implant on the basis of their strength, durability, and longevity. With the help of all the graphs and numerical computations, it has been concluded that the initial pressure for all values of k is higher for zirconia than that of titanium. Radial stresses for zirconia for all three values of k are lesser than values for titanium for all three values of k. Circumferential stresses for zirconia for all three values of k are greater than values for titanium for all three values of k. Zirconia with $k = 3$ has higher circumferential stresses and lower radial stresses than titanium. Therefore, it can be concluded that the hemispherical shell of zirconia is more compatible for the crown part of dental implant than that formed of titanium.

REFERENCES

1. Pompe, W., Worch, H., Epple, M., et al. (2008), *Functionally-graded materials for biomedical applications*, Mater. Sci. Eng.: A, 362(1-2): 40-60. doi: 10.1016/S0921-5093(03)00580-X
2. Matsuo, S., Watari, F., Ohata, N. (2001), *Fabrication of functionally graded dental composite resin post and core by laser lithography and finite element analysis of its stress relaxation effect on tooth root*, Dent. Mater. J, 20(4): 257-274. doi: 10.4012/dmj.20.257
3. Watari, F., Yokoyama, A., Omori, M., et al. (2004), *Biocompatibility of materials and development to functionally graded implant for bio-medical application*, Compos. Sci. Technol. 64 (6): 893-908. doi: 10.1016/j.compscitech.2003.09.005
4. Zou, M.-S., Jiang, L.-W., Tang, H.-C. (2022), *Computational method of underwater acoustic radiation from a spherical shell coupled with nonlinear systems*, J Sound Vibr. 533: 117020. doi: 10.1016/j.jsv.2022.117020
5. Ye, T., Jin, G., Su, Z. (2014), *Three-dimensional vibration analysis of laminated functionally graded spherical shells with general boundary conditions*, Compos. Struct. 116: 571-588. doi: 10.1016/j.compstruct.2014.05.046
6. Chu, J., Liu, X., Liu, C., et al. (2022), *Fundamental investigation of subsurface damage on the quality factor of hemispherical fused silica shell resonator*, Sensors Actuat. A: Phys. 335: 113365. doi: 10.1016/j.sna.2022.113365
7. Xu, Z., Zhu, W., Yi, G., Fan, W. (2021), *Dynamic modeling and output error analysis of an imperfect hemispherical shell resonator*, J Sound Vibr. 498: 115964. doi: 10.1016/j.jsv.2021.115964
8. Xu, Z., Yi, G., Zhu, W. (2022), *An accurate thermoelastic model and thermal output error analysis of a hemispherical resonator gyroscope under varying temperatures*, Mech. Syst. Sign. Proc. 170: 108706. doi: 10.1016/j.ymssp.2021.108760
9. Amabili, M., Breslavsky, I.D., Reddy, J.N. (2019), *Nonlinear higher-order shell theory for incompressible biological hyperelastic materials*, Comp. Meth. Appl. Mech. Eng. 346: 841-861. doi: 10.1016/j.cma.2018.09.023
10. Beheshti, A., Ansari, R. (2023), *Finite element analysis of compressible transversely isotropic hyperelastic shells*, Acta Mech. 234: 3061-3079. doi: 10.1007/s00707-023-03536-z
11. Tan, Y., He, Y., Liu, C., Li, X. (2022), *Phase field fracture model of transversely isotropic piezoelectric materials with thermal effect*, Eng. Fract. Mech. 268: 108479. doi: 10.1016/j.engfracmech.2022.108479
12. Mehta, P.D., Sahni, M., Thakur, P. (2019), *Strength analysis of functionally graded rotating disc under variable density and temperature loading*, Struct. Integr. Life, 19(2): 95-101.
13. Shi, P., Xie, J. (2023), *Exact solution of magneto-elastoplastic problem of functionally graded cylinder subjected to internal pressure*, Appl. Math. Model. 123: 835-855. doi: 10.1016/j.apm.2023.08.014
14. Kholdi, M., Saeedi, S., Moradi, S.A.Z., et al. (2022), *A successive approximation method for thermo-elasto-plastic analysis of a reinforced functionally graded rotating disc*, Arch. Civ. Mech. Eng. 22: 2. doi: 10.1007/s43452-021-00321-4
15. Bagheri, R., Ayatollahi, M., Mousavi, S.M. (2021), *Analytical solution of multiple moving cracks in functionally graded piezoelectric strip*, Appl. Math. Mech. (English Ed.) 36(6): 777-792. doi: 10.1007/s10483-015-1942-6
16. Sharma, S., Panchal, R. (2017), *Thermal creep deformation in pressurized thick-walled functionally graded rotating spherical shell*, Int. J Pure Appl. Math. 114(3): 435-444. doi: 10.12732/ijpam.v114i3.2
17. Sharma, S., Panchal, R. (2018), *Creep stresses in functionally graded rotating orthotropic cylinder with varying thickness and density under internal and external pressure*, Struct. Integr. Life, 18(2): 111-119.
18. Chand, S., Sood, S., Thakur, P., Gupta, K. (2023), *Elastoplastic stress deformation in an annular disk made of isotropic material and subjected to uniform pressure*, Struct. Integr. Life, 23(1): 61-64.
19. Godana., T.A., Singh, S.B., Thakur, P., Kumar, P. (2023), *Modelling the elastoplastic deformation of an internally pressurized transversely isotropic shell under a temperature gradient*, Turk. J Comp. Math. Educ. (TURCOMAT), 14(1): 207-221. doi: 10.17762/turcomat.v14i1.13458

20. Shahi, S. (2023), *Characterization of transitional stress concentrations in molar and premolar implants modelled as hemispherical shells under uniaxial pressure using Seth's transition theory*, Struct. Integr. Life, 23(1): 70-74.
21. Borah, B.N. (2005), *Thermo-elastic-plastic transition*, Contemp. Math. 379: 93-111. doi: 10.1090/conm/379/07027
22. Sharma, R. (2023), *Evaluation of thermal elastic-plastic stresses in transversely isotropic disk made of piezoelectric material with variable thickness and variable density subjected to internal pressure*, Struct. Integr. Life, 23(2): 205-212.
23. Sharma, R., Nagar, A. (2024), *Analytical approach on stress analysis in a functionally graded piezoelectric annular disk with varying compressibility and varying density under internal pressure*, Int. J Non-Linear Mech. 162: 104723. doi: 10.1016/j.ijnonlinmec.2024.104723

CALENDAR OF CONFERENCES, TC MEETINGS, and WORKSHOPS

March 27-28, 2025	ESIS TC8-Technical Committee on Numerical Methods and DVM Working Group Simulation Meeting	Munich, Germany	
May 18-20, 2025	ESIA18–ISSI2026 18th International Engineering Structural Integrity Assessment Conference (FESI)	University of Strathclyde, Glasgow, UK	https://fesi.org.uk/esia18-issi2026/
May 28-30, 2025	23rd Annual International Scientific Conference - Modelling in Mechanics	Ostravice, Beskydy, Czech Republic	https://www.fast.vsb.cz/228/en/mmconference/
June 23-25, 2025	TC02 - Technical Meeting in MSMF11	Brno, Czech Republic	
July 7-11, 2025	12th European Solid Mechanics Conference, Minisymposium 'Modeling fatigue of materials and structures'	Lyon, France	https://esmc2025.sciencesconf.org/resource/page/id/8
September 1-4, 2025	6th International Conference on Structural Integrity	Funchal, Madeira, Portugal	https://www.icsi.pt/
September 8-10, 2025	11th International Symposium on Fretting Fatigue (ISFF11)	Université Paris-Saclay, France	https://isff11.sciencesconf.org/?lang=en
September 11-12, 2025	IRAS 2025 - 3rd International Symposium on Risk Analysis and Safety of Complex Structures	Wrocław, Poland	https://iras2025.pwr.edu.pl/
September 15-18, 2025	IGF28 - MedFract3, 28th Int. Conf. on Fracture and Structural Integrity – 3rd Mediterranean Conf. on Fracture and Structural Integrity	Catania, Italy and web	https://www.igf28-medfract3.eu/
September 16-19, 2025	ICSID 2025 - 8th International Conference on Structural Integrity and Durability	Dubrovnik, Croatia	https://icsid2025.fsb.unizg.hr/
September 24-26, 2025	IWPDF 2025 - 4th International Workshop on Plasticity, Damage and Fracture of Engineering Materials	Istanbul, Turkey	https://iwpdf.metu.edu.tr/
November 25-28, 2025	1st Biennial ESIS-CSIC Conference on Structural Integrity	Belgrade, Serbia	https://www.beccsi2025.com/
February 18-20, 2026	ESIAM26 - The 4th European Conference on the Structural Integrity of Additively Manufactured Materials	Vicenza, Italy	
May 18-20, 2026	ESIA18–ISSI2026 18th Int. Engineering Structural Integrity Assessment Conference (ESIA18) in conjunction with China Structural Integrity Consortium's Int. Symposium on Structural Integrity 2026 (ISSI2026)	University of Strathclyde, Glasgow, UK	https://fesi.org.uk/esia18-issi2026/